

STRESS-INDUCED ANISOTROPIC POROELASTICITY RESPONSE IN SANDSTONE

David A. Lockner and Nicholas M. Beeler¹

Abstract. We present measurements of the elastic and poroelastic (both drained and undrained) properties of intact Berea sandstone at confining pressures up to 50 MPa and differential stresses from 0 to 120 MPa. Tests were carried out under axisymmetric loading conditions so that the rock developed transverse anisotropy as stress was applied. We measured the drained and undrained Young's moduli and Poisson's ratios in axial (z) and transverse (t) directions over the entire range of confining pressure and differential stress. We also directly measured the isotropic Skempton coefficient $B = (\partial p / \partial \sigma_m)_{\sigma_\Delta}$, as well as axial and transverse 'generalized' Skempton coefficients $B_t = (3/2)(\partial p / \partial \sigma_t)_{\sigma_z}$ and $B_z = 3(\partial p / \partial \sigma_z)_{\sigma_t}$. In addition we directly determined the pore space storage coefficient. The sandstone has intrinsic anisotropy at low confining pressure and stress-induced anisotropy which increases with applied differential stress due to reversible changes in pore structure. We observed significant anisotropy, with B_t as much as four times larger than B_z . Furthermore, the Biot coefficient α of the effective pressure law $\sigma_e = \sigma - \alpha p$ is not 1.0, but rather α varies systematically with stress and can be less than 0.6 at these fairly modest load conditions.

INTRODUCTION

The undrained pore pressure changes accompanying seismic faulting significantly influence Coulomb stress changes, and are generally assumed to be equal to the mean stress change. However, geologic observations show that rocks, soils, and fault zones typically have anisotropic and inhomogeneous material properties. In addition, the high differential stress commonly associated with seismic faulting can induce elastic and poroelastic anisotropy in otherwise isotropic materials. For rocks exhibiting significant elastic anisotropy, changes in differential stress $\sigma_\Delta = \sigma_1 - \sigma_3$ as well as changes in mean stress $\sigma_m = \sigma_{ii}/3$ will induce changes in pore pressure p when the rock is undrained (i.e., no fluid flow into or out of the pores). While this anisotropic response has been predicted on theoretical grounds, experimental verification has been limited. In terms of earthquake occurrence, and triggered seismicity, it is necessary to evaluate the importance of both inherent and stress-induced anisotropy in influencing pore pressure fluctuations and consequently the stabilization or destabilization of seismogenic faults.

Bedding, mineral fabric and aligned microcracks and fractures are common causes of intrinsic anisotropy in rock. These properties are often considered in discussions of anisotropic poroelastic response. However, application of deviatoric stress will also produce significant anisotropy. Stress-induced anisotropy of compressional and shear body waves in rocks is well documented (Nur and Simmons, 1969; Bonner, 1974; Lockner *et al.*, 1977; Stanchits *et al.*, 2003). Since these are the direct result of anisotropic changes in the elastic modulus tensor,

¹US Geological Survey, MS977, 345 Middlefield Road, Menlo Park, CA 94025
email: dlockner@usgs.gov, nbeeler@usgs.gov

corresponding changes in poroelastic response are implied. Direct measurement of stress-induced anisotropic poroelastic response has been limited (Wang, 1997; Lockner and Stanchits, 2002). Lockner and Stanchits (2002), hereafter referred to as *LS*, measured the undrained poroelastic response of sandstones and an unconsolidated sand pack at 20 MPa confining pressure (P_c) and 3 MPa pore pressure (p). *LS* reported an undrained pore pressure response p^u to changes in mean stress σ_m consistent with the standard definition of the pressure buildup or Skempton coefficient for isotropic materials $B = (\partial p^u / \partial \sigma_m)_{\sigma_\Delta}$ (Skempton, 1954). In addition, they observed a pore pressure response to changes in differential stress at constant mean stress $A = (\partial p^u / \partial \sigma_\Delta)_{\sigma_m}$, similar to the differential stress response A_{Skem} proposed by Skempton (1954) in his original paper. (Note that the parameter η was used by *LS* and is related to A by $A = \eta/2 = B(A_{Skem} - 1/3)$.) *LS* found that A was negative and increased approximately linearly in magnitude with increasing differential stress for the sandstones and unconsolidated sand samples. We now expand on the earlier studies, measuring drained as well as undrained poroelastic constants at effective confining pressures up to 50 MPa and differential stresses up to approximately 50% failure stress. Differential stresses were limited in this study to avoid adding a significant number of new stress-induced cracks and thereby permanently changing the elastic properties of the sample.

EXPERIMENTAL PROCEDURE

A single sample of Berea sandstone was tested in this study. The sample, cored perpendicular to bedding, was a right-cylinder with 7.62 cm diameter, 19.05 cm length and 21% porosity. Total volume and pore volume were 868.7 and 182.4 cm³, respectively. In a procedure similar to Hart and Wang (1995) two axial foil strain gages were epoxied on the sample midplane, 180° apart to measure axial strain (e_z). Two transverse strain gages also were epoxied to the midplane, again 180° apart, to measure transverse strain (e_r). The sample was jacketed in a polyurethane sleeve, clamped to steel end plugs and placed in a triaxial pressure vessel (Figure 1). Confining pressure and pore pressure were computer controlled and measured to precisions of ± 0.01 and ± 0.003 MPa, respectively. Axial load was measured using a load cell inside the pressure vessel with a precision of ± 0.02 MPa. Strain gage precision was ± 0.5 μ strain. Displacement of the piston on the pore pressure generator was monitored during drained tests (maintaining constant pore pressure). Under these conditions, movement of the pressure generator provided a direct measure of the change in pore volume of the sample during drained tests. Precision of pore volume measurements was ± 0.0005 cm³ or ± 0.6 μ strain in terms of volumetric strain. All pressures, strains and displacements were monitored and recorded at a sampling rate of 1/sec.

Undrained Tests

A series of undrained tests was carried out in which the volume of the external pore pressure system was minimized by closing an isolation valve near the sample assembly (Figure 1). In this case, the pore pressure system consisted of the sample, the pore pressure transducer and a low volume calibrated manual pressure generator. An ideal undrained test would have only the sample volume with no additional pore volume. In the *LS* study, the external pore pressure system was calibrated to determine the change in volume associated with changes in pore pressure and confining pressure. These calibrations were then used to create a virtual no-flow boundary at the sample/end-plug interface. In the present study, the sample pore volume is approximately 100

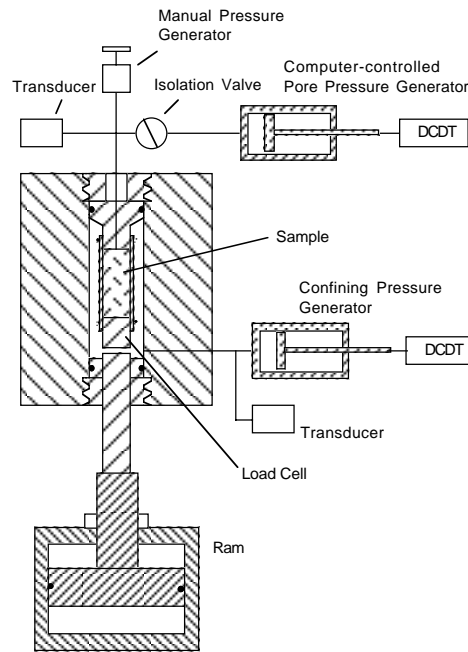


Figure 1. Test configuration showing sample in pressure vessel. Drained tests measured stress-induced pore volume changes in the sample while maintaining constant pore pressure using the computer-controlled pressure generator. Undrained tests measured pore pressure buildup with the isolation valve closed to minimize external pore pressure system volume.

times larger than in the *LS* study. Consequently, corrections for the volume of the external pore pressure system are less stringent. To determine the errors introduced by the isolated pore volume system, calibration runs were carried out using a dummy steel sample. By manually adjusting the calibrated pressure generator, the ratio of pore volume change to pore pressure change was determined. Then, by measuring changes in pore pressure in response to changes in confining pressure and axial load (using the dummy sample) the change in pore volume of the end plug and other portions of the external system could be determined. Due to the large pore volume of the test sample (182.4 cm^3), the systematic errors in determining B and A were typically ± 0.005 . Repeated measurements of the poroelastic coefficients were obtained by cycling stresses up and down by 1 to 2 MPa. Repeatability of successive measurements was typically ± 0.01 . Consequently, we have not included corrections for system volume in the undrained poroelastic measurements reported here.

All measurements were conducted at a nominal pore pressure of 10 MPa. A typical test sequence would begin by raising confining pressure and differential stress to the desired test condition, adjusting pore pressure to 10 MPa and closing the isolation valve. Then, a series of four tests was performed in which changes in pore pressure and strain were recorded in response to changes in stress components. Tests included changes in mean stress at constant differential

stress followed by changes in differential stress at constant mean stress. For the triaxial test geometry, $\sigma_x = \sigma_y = P_c$, and a second pair of tests was carried out imposing changes in σ_z at constant P_c , and changes in P_c at constant σ_z . Given the transverse symmetry in the applied stress field achievable in the triaxial test geometry, the σ_m/σ_Δ test and σ_z/P_c test represent redundant pairs of measurements for determining the undrained poroelastic response. For each test sequence, the control stress variable was cycled up and down twice by 1 to 3 MPa to obtain repeated measurements of the pore pressure response. In many cases, the first half cycle in loading included a component of irreversible pore pressure response. For this reason, only the second, third and fourth half cycle measurements were used in determining the reversible elastic response. (See (Lockner and Stanchits, 2002) for a more detailed description of this effect.) This irreversible component in the pore pressure response was found to occur even though the sample had initially been ‘pre-conditioned’ (see, for example, (Hart and Wang, 1995)) by raising confining pressure and stress to a level higher than any of the stresses used during the main sequence of tests. Over the course of the experiment, tests were repeated at 20 MPa confining pressure and differential stresses of 0 and 10 MPa to check for permanent changes in the poroelastic response due to stress cycling. Pore pressure responses were consistent to within the experimental error, indicating that irreversible damage accumulated during the entire experiment must be small.

Drained Tests

A second series of drained tests was carried out in which pore pressure was held constant while the sample was subjected to different stress paths. Again, imposed stress paths included changes in mean stress at constant differential stress, changes in differential stress at constant mean stress, changes in σ_z at constant P_c and changes in P_c at constant σ_z . During these tests, changes in strain and pore volume were measured. The σ_m/σ_Δ test and σ_z/P_c test represent redundant pairs of measurements for determining the drained poroelastic response.

Compressibility Test

A final test was conducted at each applied stress state to measure sample compressibility. With the isolation valve closed, the calibrated pressure generator was adjusted by 0.040 cm³ (45 μ strain in volume) and the changes in p , e_t and e_z were recorded.

RESULTS

Axisymmetric Poroelasticity

Results are presented using the formalism of Cheng (1997). We will use ‘‘engineering notation’’ in which stresses and strains are expressed as

$$\underline{\sigma} = [\sigma_x \quad \sigma_y \quad \sigma_z \quad \tau_x \quad \tau_y \quad \tau_z]^T \quad (1)$$

$$\underline{e} = [e_x \quad e_y \quad e_z \quad \gamma_x \quad \gamma_y \quad \gamma_z]^T. \quad (2)$$

Then, the constitutive equations for linear poroelasticity can be expressed as

$$\underline{\sigma} = \underline{\underline{M}}\underline{e} - \alpha p \quad (3)$$

$$p = M(\zeta - \underline{\alpha}^T \underline{e}) \quad (4)$$

where \underline{M} is the drained stiffness matrix (equivalent to the familiar Hooke's law moduli), $\underline{\alpha}$ represents the generalized Biot effective stress coefficients (Biot and Willis, 1957), ζ is the fluid mass flow out of the sample, and the parameter M is related to bulk modulus. The inverse form of (3) and (4) gives the constitutive equations in terms of the compliance matrix \underline{C} :

$$\underline{e} = \underline{C}\underline{\sigma} + \frac{C}{3}\underline{B}p \quad (5)$$

$$\zeta = C\left(p + \frac{1}{3}\underline{B}^T \underline{\sigma}\right). \quad (6)$$

In this case, \underline{B} represents the generalized Skempton coefficients and C is a storage coefficient. The constitutive equations apply to linear, or at least incrementally linear, poroelasticity. For stress-induced anisotropy, which dominates the poroelastic behavior reported here, poroelastic coefficients vary continuously with stress state. In this case, the constitutive equations (3) through (6) are understood to relate small changes in strain and fluid pressure to incremental stress variations about some ambient stress state.

The triaxial test geometry imposes a radial or transverse symmetry on the stress and strain fields occurring in our experiments. In this case, the 28 independent constitutive coefficients needed to characterize fully anisotropic poroelasticity in equations (3) through (6) are reduced to eight. Cheng (1997) provides formulas for expressing the drained stiffness tensor coefficients in terms of drained Young's moduli in the transverse plane of symmetry $E_t = E_x = E_y$, and parallel to the sample axis E_z , and two Poisson's ratios ν_t and ν_z . The Poisson ratio ν_t represents the contraction in the plane of symmetry perpendicular to a tensile stress applied in the plane of symmetry. Similarly, ν_z represents the contraction in the plane of symmetry resulting from a tensile stress applied axially. For a transversely isotropic system, \underline{M} is composed of

$$\underline{\underline{M}} = \begin{bmatrix} M_{11} & M_{12} & M_{13} & 0 & 0 & 0 \\ M_{12} & M_{11} & M_{13} & 0 & 0 & 0 \\ M_{13} & M_{13} & M_{33} & 0 & 0 & 0 \\ 0 & 0 & 0 & G & 0 & 0 \\ 0 & 0 & 0 & 0 & G' & 0 \\ 0 & 0 & 0 & 0 & 0 & G' \end{bmatrix} \quad (7)$$

where $G = (M_{11} - M_{12})/2$ and individual terms are expressed as

$$M_{11} = \frac{E_t^2(E_z - E_t\nu_z^2)}{\Lambda} \quad (8)$$

$$M_{12} = \frac{E_t^2(E_z\nu_t + E_t\nu_z^2)}{\Lambda} \quad (9)$$

$$M_{13} = \frac{E_t^2 E_z (v_z + v_t v_z)}{\Lambda} \quad (10)$$

$$M_{33} = \frac{E_z^2 E_t (1 - v_t^2)}{\Lambda} \quad (11)$$

with

$$\Lambda = E_t (1 + v_t) (E_z - E_z v_t - 2E_t v_z^2). \quad (12)$$

The four parameters E_z , E_t , v_z , and v_t can be determined from strain gage response to independent application of axial load and confining pressure. Determination of G' would require, for example, application of a shear stress in the axial direction and cannot be achieved by static loading in a standard triaxial system. Consequently, we have computed four of the five independent elements of the stiffness matrix by applying incremental stress cycles under drained (constant pore pressure) conditions.

The compliance matrix can be written explicitly as

$$\underline{\underline{C}} = \begin{bmatrix} 1/E_t & -v_t/E_t & -v_z/E_z & 0 & 0 & 0 \\ -v_t/E_t & 1/E_t & -v_z/E_z & 0 & 0 & 0 \\ -v_z/E_z & -v_z/E_z & 1/E_z & 0 & 0 & 0 \\ 0 & 0 & 0 & 1/G & 0 & 0 \\ 0 & 0 & 0 & 0 & 1/G' & 0 \\ 0 & 0 & 0 & 0 & 0 & 1/G' \end{bmatrix}. \quad (13)$$

Other coefficients become

$$\underline{\alpha} = [\alpha_t \quad \alpha_t \quad \alpha_z \quad 0 \quad 0 \quad 0]^T \quad (14)$$

$$\underline{B} = [B_t \quad B_t \quad B_z \quad 0 \quad 0 \quad 0]^T \quad (15)$$

with

$$\alpha_t = 1 - \frac{M_{11} + M_{12} + M_{13}}{3K_s} \quad (16)$$

$$\alpha_z = 1 - \frac{M_{33} + 2M_{13}}{3K_s} \quad (17)$$

$$B_t = \frac{3(C_{11} + C_{12} + C_{13}) - C_s}{C} \quad (18)$$

$$B_z = \frac{3(C_{33} + 2C_{13}) - C_s}{C}. \quad (19)$$

For a monomineralic matrix, $K_s = 1/C_s$ represents the bulk modulus of the matrix constituent. For isotropic samples this is typically determined from an ‘unjacketed’ pressure test in which $P = P_c = p$ according to $K_s = -P/e$. The storage coefficient C is given by

$$C = (C^* - C_s) + \phi(C_f - C_s) \quad (20)$$

with

$$C^* = 2C_{11} + C_{33} + 2C_{12} + 4C_{13}, \quad (21)$$

ϕ is porosity and $C_f = 1/K_f$, where K_f is the fluid bulk modulus.

Drained Tests

Two examples of the stiffness matrices are presented demonstrating the development of anisotropy as differential stress was applied to the sample. Matrix components are computed from strain gage response in drained tests (pore pressure held constant at 10 MPa) according to equations (8) through (12). Tests were conducted at an ambient confining pressure of 30 MPa and differential stresses of 10 and 70 MPa, respectively. Failure stress of Berea sandstone at this effective confining pressure is 140 MPa. Matrix components are expressed in GPa.

$$\underline{\underline{M}}|_{\sigma_3=10MPa} = \begin{bmatrix} 20.00 & 4.01 & 4.85 & 0 & 0 & 0 \\ 4.01 & 20.00 & 4.85 & 0 & 0 & 0 \\ 4.85 & 4.85 & 22.27 & 0 & 0 & 0 \\ 0 & 0 & 0 & 8.00 & 0 & 0 \\ 0 & 0 & 0 & 0 & ? & 0 \\ 0 & 0 & 0 & 0 & 0 & ? \end{bmatrix} \quad (22)$$

$$\underline{\underline{M}}|_{\sigma_3=70MPa} = \begin{bmatrix} 17.34 & 3.10 & 4.84 & 0 & 0 & 0 \\ 3.10 & 17.34 & 4.84 & 0 & 0 & 0 \\ 4.84 & 4.84 & 29.42 & 0 & 0 & 0 \\ 0 & 0 & 0 & 7.12 & 0 & 0 \\ 0 & 0 & 0 & 0 & ? & 0 \\ 0 & 0 & 0 & 0 & 0 & ? \end{bmatrix} \quad (23)$$

At 10 MPa load, the sample has developed a modest anisotropy which increases significantly as load is increased. For example, the ratio M_{11}/M_{33} drops from 0.90 at 10 MPa to 0.59 at 70 MPa (50% failure stress). These changes in moduli would result in a decrease in the ratio of slow (transverse) to fast (axial) P wave speed from 0.95 to 0.77. Young’s moduli and Poisson’s ratios for drained tests at confining pressures of 20 and 60 MPa are plotted in Figure 2. Increasing confining pressure has two primary effects. First, the rock matrix is stiffened, increasing the moduli. Second, increased confining pressure tends to suppress anisotropy. These measurements were all conducted below 50% failure stress so that the trends here are reversible. We verified the reversibility of the measurements by periodically repeating measurements at $P_c = 20$ MPa and $\sigma_\Delta = 0$ and 10 MPa. If tests had been extended to higher differential stress, new microcrack damage would have been introduced in the sample resulting in significantly larger anisotropy (Lockner *et*

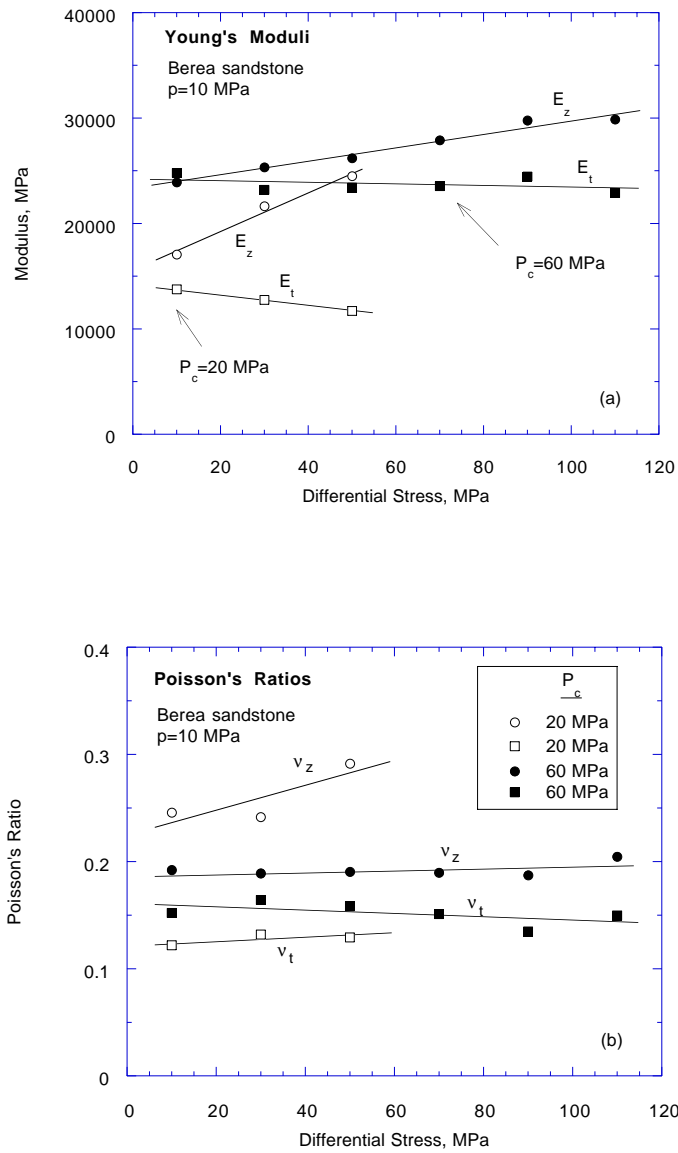


Figure 2. (a) Changes in axial (E_z) and transverse (E_t) Young's moduli in response to increasing differential stress during drained tests. Pore pressure was 10 MPa. Confining pressures were 20 and 60 MPa. Failure strengths at these effective confining pressures were 140 and 224 MPa, respectively. (b) Corresponding measurements of Poisson's ratios. Increased confining pressure reduces anisotropy while increased differential stress increases anisotropy.

al., 1977; Lockner and Stanchits, 2002).

Biot's effective pressure coefficients α can now be calculated using equations (16) and (17). We use $K_s = 30GPa$ which is an average value of solid constituent bulk modulus reported by Hart and Wang (1995) for a suite of five Berea sandstone samples. The result, plotted in Figure 3,

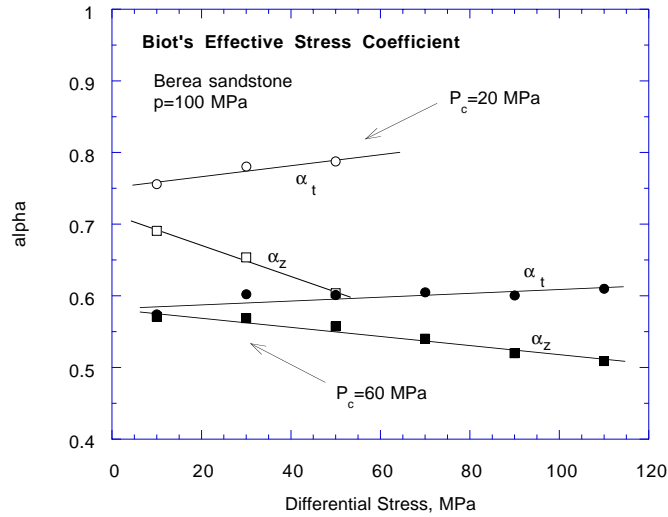


Figure 3. Biot’s generalized effective pressure coefficient $\underline{\alpha}$, defined by $\underline{\sigma}_e = \underline{\sigma} + \underline{\alpha}p$. Coefficients α_t and α_z were calculated from data in Figure 2 using (16) and (17).

shows a pronounced dependence of $\underline{\alpha}$ on both confining pressure and differential stress. At higher confining pressure, the pore pressure contribution to effective pressure is diminished and the overall anisotropy in the Biot coefficients is suppressed. At low differential stress, the Biot coefficient for Berea sandstone is nearly isotropic ($\alpha_t \cong \alpha_z$). Increasing differential stress results in a linear increase in anisotropy over the range of measurements reported here.

Undrained Tests

In this section we show results for incremental stress cycling tests of the Berea sandstone sample under undrained conditions. In this case, fluid trapped in the pores will respond to stress changes as the pore space compresses or dilates. The principal measure of undrained poroelastic response is the generalized Skempton or pressure build up coefficient \underline{B} appearing in constitutive equations (5) and (6). For the fully anisotropic material, \underline{B} is comprised of six independent coefficients. However, the transversely isotropic symmetry imposed by the triaxial loading geometry reduces the independent coefficients to two (equation (15)); representing axial and transverse sensitivity. It is possible to calculate \underline{B} by combining elasticity measurements from drained tests with determinations of compliances of the pore fluid and solid matrix (see, for example, equations (18) through (21)). First, we show results from the direct measurement of pore pressure buildup during undrained tests. Skempton coefficients are determined directly from equation (6) by applying a no-flow condition ($\zeta = 0$), which in the case of transverse symmetry leads directly to

$$dp^u = -\frac{1}{3}(2B_t dP_c + B_z d\sigma_z). \tag{24}$$

Here we have written the pressure change as a differential since the poroelastic coefficients vary with pressure and stress and the governing equations are only incrementally linear. Skempton

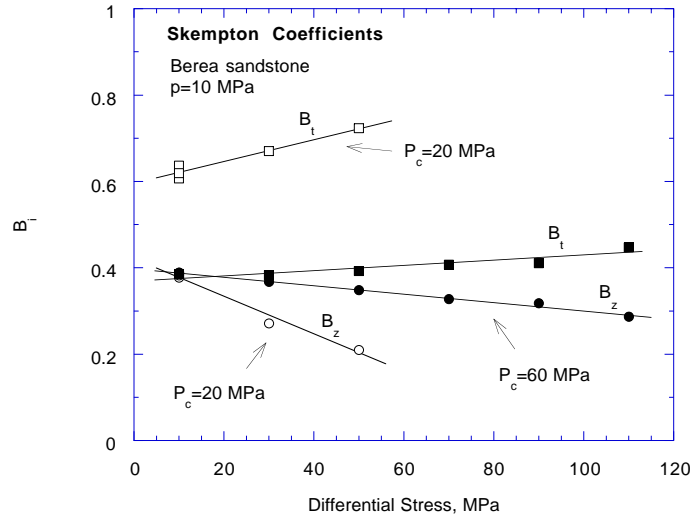


Figure 4. Generalized Skempton coefficients B_t and B_z measured directly in undrained tests by recording the pore pressure buildup according to equation (24).

coefficients are determined at a given stress state from two tests: varying axial stress at constant confining pressure and varying confining pressure at constant axial stress. Results for tests at 10 MPa pore pressure and ambient confining pressures of 20 and 60 MPa are shown in Figure 4. At low confining pressure and low differential stress B_z and B_t differ by about 30%, indicating an intrinsic anisotropy in this sample. Increasing confining pressure erases the intrinsic anisotropy by decreasing B_z . Similar to the other coefficients, anisotropy of the Skempton coefficient increased with increasing differential stress.

Three independent methods of determining standard Skempton coefficient $B = \left(\partial p^u / \partial \sigma_m \right)_{\sigma_\Delta}$ are plotted in Figure 5 to test the self consistency of the system of measurements presented here. Solid circles and squares show determinations of B from direct undrained measurements in which mean stress was varied at constant differential stress. Uncertainties are estimated as ± 0.01 . The scalar coefficient B shows minor sensitivity to increasing differential stress. However, the stiffening effect of increasing confining pressure reduces B from 0.56 to 0.39. Open circles and squares show estimates of B as calculated from undrained pore pressure measurements of B_z and B_t . Pore pressure changes are then predicted according to equation (24) using the constraint that $d\sigma_m|_{\sigma_\Delta=const} = (2dP_c + d\sigma_z)/3$. Uncertainties in these calculations are approximately ± 0.015 . The final determination of B comes from the strain measurements during drained tests. In this case, the compliance matrix is calculated from stress tests at constant pore pressure according to equation (13). Then B_z and B_t are estimated using equations (18) through (21). Finally, B is calculated according to (24) and plotted in Figure 5 as solid triangles. Uncertainties are estimated to be ± 0.02 . At 60 MPa confining pressure, both estimates of B coincide well with the direct measurements. At 20 MPa confining pressure, estimates of B derived from strain measurements during tests differ from direct measurements of B by up to 7%. In one sense, it is remarkable that this procedure, estimating pore pressure buildup from measurements made without any pore

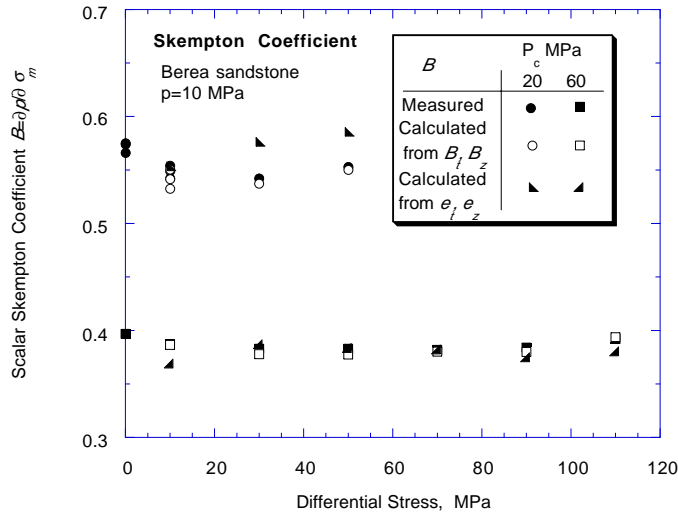


Figure 5. Standard Skempton pore pressure buildup coefficient B plotted versus differential stress. Three independent determinations of B are shown: Solid circles and squares are direct measurements of undrained pore pressure change at constant differential stress; open circles and squares show B calculated from undrained pore pressure measurements of B_t and B_z ; solid triangles show B calculated from strain measurements under drained conditions.

pressure interaction, are this successful. This comparison represents a test of a number of fundamental assumptions used in the development of poroelasticity theory regarding, for example, assumptions of micro-homogeneity and micro-isotropy (Cheng, 1997).

Storage Coefficients

A parameter often used by hydrogeologists is storativity S (Cheng, 1997) or one-dimensional storage coefficient (Green and Wang, 1990; Hart and Wang, 1995), expressed as $S = \zeta/p|_{e_x=e_y=e_z=0}$. This coefficient relates the amount of fluid that can be extracted from a porous medium under the conditions of constant overburden stress and uniaxial compaction. Now consider equation (6) under the stress boundary condition: $\underline{B}^T \underline{\sigma} = 0$. Upon rewriting, we see that $C = \zeta/p|_{\underline{B}^T \underline{\sigma} = 0}$ and C is also a storage coefficient. In particular, C is the storage coefficient associated with constant stress ($\underline{\sigma} = 0$) boundary conditions and is referred to as the three-dimensional storage coefficient by Hart and Wang (1995). We have measured C directly under constant stress conditions by measuring the pore pressure drop resulting from removal of 0.040 cm³ water from the sample. In these tests, the pore pressure drop was on the order of 1 MPa. In addition to the direct measurement, C was calculated using strain gage variations under drained conditions according to equation (20). All measurements were made at a nominal pore pressure of 10 MPa. The storage coefficient was determined to be relatively insensitive to differential stress. Consequently, we report average values at two confining pressures. For $P_c = 20$ MPa, $C_{measured} = (1.88 \pm 0.10) \times 10^{-4}$

MPa⁻¹ and $C_{calc} = (1.80 \pm 0.14) \times 10^{-4}$ MPa⁻¹. For $P_c = 60$ MPa, $C_{measured} = (1.34 \pm 0.06) \times 10^{-4}$ MPa⁻¹ and $C_{calc} = (1.24 \pm 0.04) \times 10^{-4}$ MPa⁻¹. Uncertainties represent two standard deviations. The estimates of the storage coefficient based on drained rock compliances agreed with the directly measured values to within 8%.

Next, consider uniaxial compaction under constant overburden stress for transverse symmetry in the horizontal plane. For these boundary conditions, we can compare S and C directly. Equation (6) becomes

$$S = \left. \frac{\zeta}{p} \right|_{e_t = \sigma_z = 0} = C + \frac{2}{3} CB_t \frac{\sigma_t}{p}. \quad (25)$$

Application of the boundary conditions to equation (5) and substitution into (25) gives

$$S = \left. \frac{\zeta}{p} \right|_{e_t = \sigma_z = 0} = C - \frac{\left(C_{11} + C_{12} + C_{13} - \frac{C_s}{3} \right)^2}{C_{11} + C_{12}}. \quad (26)$$

For $P_c = 20$ MPa, $S_{calc} = (1.20 \pm 0.12) \times 10^{-4}$ MPa⁻¹, and for $P_c = 60$ MPa, $S_{calc} = (1.07 \pm 0.04) \times 10^{-4}$ MPa⁻¹. We have already noted that increasing confining pressure reduces the compliance of the rock framework. This same stiffening effect reduces the magnitude of the storage coefficients as well.

CONCLUSIONS

Through the combined measurements of strain and pore pressure changes in response to specific incremental stress paths, we have determined anisotropic poroelastic coefficients for Berea sandstone. At low confining pressure, Berea sandstone has a small component of intrinsic anisotropy. Increasing confining pressure stiffens the rock matrix and eliminates the intrinsic anisotropy. At all confining pressures tested, application of differential stress produced increased anisotropy approximately proportional to the applied load. By limiting differential stress to less than 50% failure stress, the amount of new, irreversible microcrack damage added to the sample was minimized. Consequently, the stress-induced anisotropy that we observed was reversible and the sample reverted to nearly its initial state upon removal of stress. These observations provide new experimental confirmation of the theory of incremental linear anisotropic poroelasticity as well as direct measurement of stress-induced anisotropic poroelastic response of rock.

The assumption of isotropy implies that four independent constitutive material properties are needed to properly represent poroelastic systems. While this small number of constitutive constants is desirable, there are many natural examples in which materials are clearly anisotropic. Bedding and fabric are two obvious examples. In this paper we have shown that rocks that would normally be isotropic become increasingly anisotropic as deviatoric stress is applied. Not only is this true near the yield stress, but even at lower deviatoric stress levels, where rocks remain within their elastic limit, stress-induced anisotropy can be significant. Regions in which seismic shear wave splitting is observed will also exhibit anisotropy in poroelastic properties. These include, for example, regions containing active faults. The simplest anisotropic system, tested in this study, contains a plane of symmetry. Eight independent poroelastic constants are needed to characterize this transversely isotropic system. The inherent increase in complexity may be

necessary to properly model such diverse problems as basin evolution and fault interactions.

Acknowledgements. We thank D. Moore and E. Roeloffs for helpful reviews of this manuscript. This work was supported by the National Earthquake Hazards Reduction Program.

REFERENCES

- Biot, M. A., and D. G. Willis (1957). The elastic coefficients of the theory of consolidation, *J. Appl. Mech., Trans. ASME*, **79**, 596-601.
- Bonner, B. P. (1974). Shear wave birefringence in dilating granite, *Geophys. Res. Lett.*, **1**, 5, 217-220.
- Cheng, A. H.-D. (1997). Material coefficients of anisotropic poroelasticity, *Int. J. Rock Mech. Min. Sci. Geomech. Abstr.*, **34**, 2, 199-205.
- Green, D. H., and H. F. Wang (1990). Specific storage as a poroelastic coefficient, *Water Resour. Res.*, **26**, 1631-1637.
- Hart, D. J., and H. F. Wang (1995). Laboratory measurements of a complete set of poroelastic moduli for Berea sandstone and Indiana limestone, *J. Geophys. Res.*, **100**, 17,741-17,751.
- Lockner, D. A., and S. A. Stanchits (2002). Undrained poroelastic response of sandstones to deviatoric stress change, *J. Geophys. Res.*, **107**, B12, 2353, doi:10.1029/2001JB001460.
- Lockner, D. A., J. B. Walsh, and J. D. Byerlee (1977). Changes in seismic velocity and attenuation during deformation of granite, *J. Geophys. Res.*, **82**, 33, 5374-5378.
- Nur, A., and G. Simmons (1969). Stress-induced velocity anisotropy in rock: An experimental Study, *J. Geophys. Res.*, **74**, 27, 6667-6674.
- Skempton, A. W. (1954). The pore-pressure coefficients A and B, *Geotechnique*, **4**, 143-147.
- Stanchits, S. A., D. A. Lockner, and A. V. Ponomarev (2003). Anisotropic changes in P-wave velocity and attenuation during deformation and fluid infiltration of granite, *Bull. Geol. Soc. Amer.*, in press.
- Wang, H. F. (1997). Effects of deviatoric stress on undrained pore pressure response to fault slip, *J. Geophys. Res.*, **102**, 17,943-17,950.